Clim. Past, 8, 415–431, 2012
www.clim-past.net/8/415/2012/
doi:10.5194/cp-8-415-2012

Climate of the Past

Climatically-controlled siliceous productivity in the eastern Gulf of Guinea during the last 40 000 yr

X. Crosta[1], O. E. Romero[2], O. Ther[1], and R. R. Schneider[3]

[1]CNRS/INSU, UMR5805, EPOC, Université Bordeaux 1, Talence Cedex, France
[2]Instituto Andaluz de Ciencias de la Tierra (CSIC-UGR), 18100 Armilla-Granada, Spain
[3]Marine Klimaforschung, Institut fuer Geowissenschaften, CAU Kiel, Germany

Correspondence to: X. Crosta (x.crosta@epoc.u-bordeaux1.fr)

Received: 30 June 2011 – Published in Clim. Past Discuss.: 25 July 2011
Revised: 27 January 2012 – Accepted: 30 January 2012 – Published: 7 March 2012

Abstract. Opal content and diatom assemblages were analysed in core GeoB4905-4 to reconstruct siliceous productivity changes in the eastern Gulf of Guinea during the last 40 000 yr. Opal and total diatom accumulation rates presented low values over the considered period, except during the Last Glacial Maximum and between 15 000 calendar years Before Present (15 cal. ka BP) and 5.5 cal. ka BP, the so-called African Humid Period, when accumulation rates of brackish and freshwater diatoms at the core site were highest. Conversely, accumulation rates of windblown diatoms exhibited an opposite pattern with higher values before and after the African Humid Period and greatest values during Heinrich Events, the Younger Dryas and since 5.5 cal. ka BP.

Our results demonstrate that siliceous productivity in the eastern Gulf of Guinea was directly driven by the nutrient load from local rivers, whose discharges were forced by precipitation changes over western Equatorial Africa and/or modification of the fluvio-deltaic systems forced by sea level changes. Precipitation in this region is controlled by the West African monsoon which is, in turn, partly dependent on the presence and intensity of the Atlantic Cold Tongue (ACT). Our results therefore suggest that the ACT was weakened, warmer trade winds were less vigorous, and cloud convection and precipitation were greater during the AHP though centennial-to-millennial timescale dry events were observed at ∼10 cal. ka BP, ∼8.5 cal. ka BP and ∼6 cal. ka BP. Conversely, the ACT was more intense, trade winds were more vigorous and African climate was more arid during H1, the Younger Dryas and after 5.5 cal. ka BP into the present.

1 Introduction

A substantial part of the ocean's primary productivity is supported by diatoms (Tréguer et al., 1995). At the global ocean scale, diatom productivity primarily depends on the availability of dissolved silica (DSi) as diatoms need DSi to build their frustule. This explains why diatoms are dominant in the Southern Ocean, the North Pacific, coastal zones, and low-latitude upwelling systems where high stocks of DSi prevail. Dissolved silica stocks in coastal zones mainly result from sediment remobilisation and riverine input, while DSi stocks in the North Pacific, Southern Ocean and upwelling systems are a consequence, at first order, of the marine silica cycle and global ocean circulation (Ragueneau et al., 2000). Conversely, diatoms are less competitive in oligotrophic tropical gyres where high sea-surface temperatures and low DSi stocks limit silica uptake by diatoms (Hildebrand, 2000; Martin-Jézéquel et al., 2000).

Diatom production and burial in the Gulf of Guinea, defined as the part of the Atlantic Ocean northeast of a line running from Liberia to Gabon, are relatively low. Abundances hardly reach 1.10^7 diatoms per gram in surface sediments (Romero and Armand, 2010), which is 1–2 order of magnitude lower than diatom occurrences in the Southern Ocean (Crosta et al., 1997) and coastal upwellling systems (Romero et al., 2002; Abrantes et al., 2007). Diatom abundances in surface sediments of the Gulf of Guinea additionally demonstrate a westward decreasing gradient (Pokras and Molfino, 1986), in phase with the westward increasing gradient in salinity (Weldeab et al., 2007a). Such distribution is related to low mean DSi concentrations in surface waters

with values of ∼2.5 µM in the western part of the Gulf of Guinea where DSi stocks originate from the nutrient-poor South Atlantic Central waters transported by the South Equatorial Counter Current (Peterson and Stramma, 1991) and ∼8 µM in the eastern part of the Gulf of Guinea where rivers inject nutrient-rich freshwaters (Hughes et al., 2011). There is therefore a direct connection between DSi stocks and diatom production in surface waters and occurrence in sediments of the Gulf of Guinea and precipitation regimes over western Equatorial Africa.

Past changes in siliceous productivity were reconstructed on glacial-interglacial timescale in the east Equatorial Atlantic and the Congo Fan from the southeast Atlantic. In the east Equatorial Atlantic, variations in siliceous productivity and marine diatom assemblages were mainly related to the intensity of the equatorial upwelling in response to changes in the intensity and direction of the trade winds (Abrantes et al., 2003). In the southeast Atlantic off the Congo River, variations in siliceous productivity and marine diatom assemblages were related to the interplay of riverine discharges, in turn controlled by changes in precipitation in western and central Equatorial Africa, and migrations of oceanic fronts, controlled by changes in wind regimes (Uliana et al., 2002; Marret et al., 2008).

Because of the absence of upwelling (Stramma and England, 1999) and proximity to the ITCZ, the eastern Gulf of Guinea may provide more straightforward information on climate changes in western Equatorial Africa than the eastern Equatorial Atlantic and the Congo Fan. Past changes in siliceous productivity there have been linked to local river discharges, forced by precipitation regime over western Equatorial Africa, though no real evidenced was provided (Weldeab et al., 2005, 2007b). Indeed, downcore records of diatom assemblages have never been produced for the eastern Gulf of Guinea. We here present diatom assemblages in core GeoB4905-4 to compliment the existing record of opal content (Weldeab et al., 2007a), located around 115 km to the southwest of the Sanaga River mouth, to assess (1) the dependency of diatom productivity to DSi delivered by local rivers to the ocean and (2) climate changes, i.e. precipitation and wind regimes over the central African continent during the last 40 000 yr at the centennial scale resolution.

2 Oceanographic and climatic settings

The sea-surface circulation in the Equatorial Atlantic, driven by the atmospheric surface circulation, is governed by the North Equatorial Counter Current (NECC) that transports South Atlantic Central waters (SACW) towards the east (Stramma and England, 1999). SACW, which are the main surface to sub-surface water mass in the South Atlantic, are low nutrient and saline waters that extend until ∼500 m deep (Peterson and Stramma, 1991). The NECC is relayed by the Guinea Current (GC) that advects the low nutrient, saline waters into the Gulf of Guinea (Fig. 1). The GC is stronger during the boreal summer than the boreal winter. Surface waters exit to the south as the Angola Current (AC). Eventually, the AC transports southward a mix of warm, nutrient-poor surface waters and cool, upwelled waters from the Equatorial Under-Current (EUC) until the Angola-Benguela Front where it meets, at around 15° S, the northward surface drift from the Cape Basin.

The Niger and Sanaga Rivers are the two main rivers flowing in the eastern Gulf of Guinea. They cover a catchment area of $\sim 2\,400\,000\,km^3\,yr^{-1}$ and drive an annual riverine freshwater input of $\sim 277\,km^3$ (Weldeab et al., 2007a). More particularly, the drainage area of the Sanaga River is $133\,000\,km^2$ and the mean annual discharge is $62\,km^3\,yr^{-1}$(Kossoni et al., 2010). River discharges are minimal during the boreal winter–spring (February–April) and maximal during the boreal summer–autumn (July–November), with peak runoffs in September and October (Weldeab et al., 2007a; Kossoni et al., 2010). Annual variations in the Sanaga discharge are determined by the yearly cycle of precipitations over Equatorial Africa, controlled by the West African monsoon (WAM). Atmospheric surface circulation in the Gulf of Guinea is dominated all year round by southwesterly trade winds (TW), which provide most of the moisture for the WAM (Lebel et al., 2009). The quantity of moisture available for the WAM is partly determined by the sea-surface temperature gradient between tropics and subtropics and, thus, the presence and extent of the Atlantic Cold Tongue (ACT) in the subtropical south Atlantic (Ruiz-Barradas et al., 2000). Warm sea-surface temperature anomalies in the Gulf of Guinea lead to greater evaporation and water vapour in the lower troposphere that, in turn, conducts to greater precipitation along the Guinean Coast (Tokinaga et al., 2011). From a large-scale perspective, the WAM can be described in terms of the annual migration of the Inter-Tropical Convergence Zone (ITCZ). The ITCZ is located around 5–10° N and 15–20° N in western Equatorial Africa during the boreal winter and boreal summer, respectively, in response to the northward migration of the maximum of received solar radiation energy. Large precipitation over western Equatorial Africa, around $3000\,mm\,yr^{-1}$ (Kossoni et al., 2010), support the presence of evergreen rainforest and savannah (Foley et al., 2003).

Dissolved silica in surface waters of the southwest Atlantic Ocean are around 2.5 µM (World Ocean Atlas, 2001) and, thus, bring very little nutrient to the eastern Gulf of Guinea. Dissolved silica concentrations in surface waters of the eastern Gulf of Guinea are slightly higher than in the open ocean with values of ∼6–8 µM during the boreal summer (July–October) and ∼2 µM during the boreal winter-spring (March–June) (World Ocean Atlas, 2001). These variations appear related to the yearly cycle of discharge of local rivers that present mean concentrations of $\sim 15\,mg\,l^{-1}$ or ∼230 µM (Boeglin et al., 2003; Hughes et al., 2011). High dissolved silica concentrations in African rivers are related to

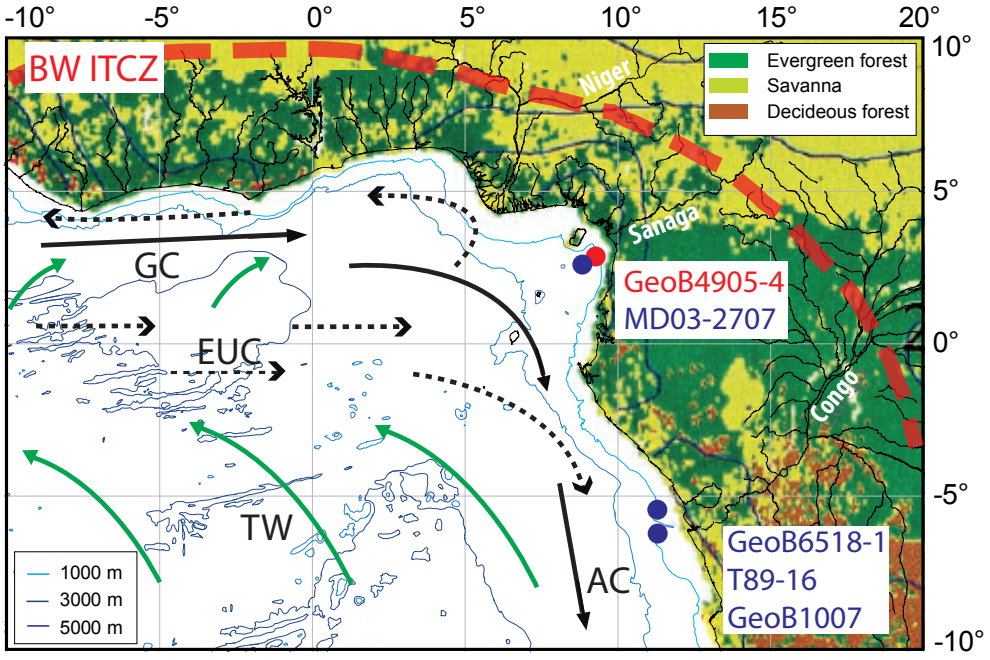

Fig. 1. Bathymetric map of the Gulf of Guinea displaying location of core GeoB4905-4 and other reference sites, along with main surface (plain black arrows) and subsurface currents (dashed black arrows), main atmospheric circulation (green arrows), position of the boreal winter ITCZ (red dashed line), main rivers flowing into the Gulf of Guinea and vegetation distribution in western Equatorial Africa (Foley et al., 2003). The boreal summer ITCZ is located around 15–20° N (not in figure). GC: Guinea Current; AC: Angola Current; EUC: Equatorial Undercurrent; TW: Trade Winds.

the prevalence of warm climate conditions that favour chemical weathering of crystalline rocks abundant on this continent (Dürr et al., 2011). Monitoring of Sanaga River discharge, dissolved silica content and chlorophyll-a concentration in surface waters of the eastern Gulf of Guinea during the year 2005 evidenced a strong relationship between DSi brought to the ocean by riverine fresh water discharge and local productivity (Weldeab et al., 2007a).

3 Material and methods

3.1 Stratigraphy

Gravity core GeoB4905-4 was retrieved during the Meteor cruise M41/1 in the eastern Gulf of Guinea (2°30′ N, 9°23.4′ E, 1328 m of water depth) around 115 km to the southwest of the Sanaga River mouth (Fig. 1). The age model of core GeoB4905-4 was published by Adegbie et al. (2003) and Weldeab et al. (2005). Briefly, it is based on fourteen ^{14}C-AMS dates of monospecific samples of the planktonic foraminifer *Globigerinoides ruber* pink and mixed planktonic foraminifers for the upper 9 m of the core. Additional tuning points between the δ^{18}O *G. ruber* pink record and GISP2 δ^{18}O record allowed extention of the stratigraphy beyond the radiocarbon range. Radiocarbon ages were corrected for the mean marine reservoir age and calibrated to calendar ages using CALIB5 (Stuiver et al., 2005). The core covers the last 45 000 calendar years (cal. ka BP) in 1218 cm.

3.2 Diatom analysis

Diatom slides were prepared following the protocol outlined in Rathburn et al. (1997). Diatom identification was achieved on a Nikon 80i phase contrast microscope at a magnification of × 1000. A minimum of 300 valves were identified, whenever possible, following the counting rules described in Crosta and Koç (2007). Several traverses across the coverslip were performed, depending on valve adundances. Three cover slips per samples were examined. It was not possible to reach 300 diatom valves in samples between 12.5–13.3 cal. ka BP and 14.8–17.1 cal. ka BP.

Diatoms were identified to species or species group level, and the relative abundance of each species was determined as the fraction of the diatom species against total diatom abundance in the sample. Identification of marine diatoms was based on Sundström (1986), Moreno-Ruiz and Licea (1994), Moreno et al. (1996), Hasle and Syversten (1997), Romero et al. (1999), Rivera et al. (2006) and a suite of species-specific references. Identification of brackish and freshwater diatoms was based on Servant-Vildary (1981), Gasse (1986), Lange and Tiffany (2002), Sar et al. (2010) and a suite of species-specific references.

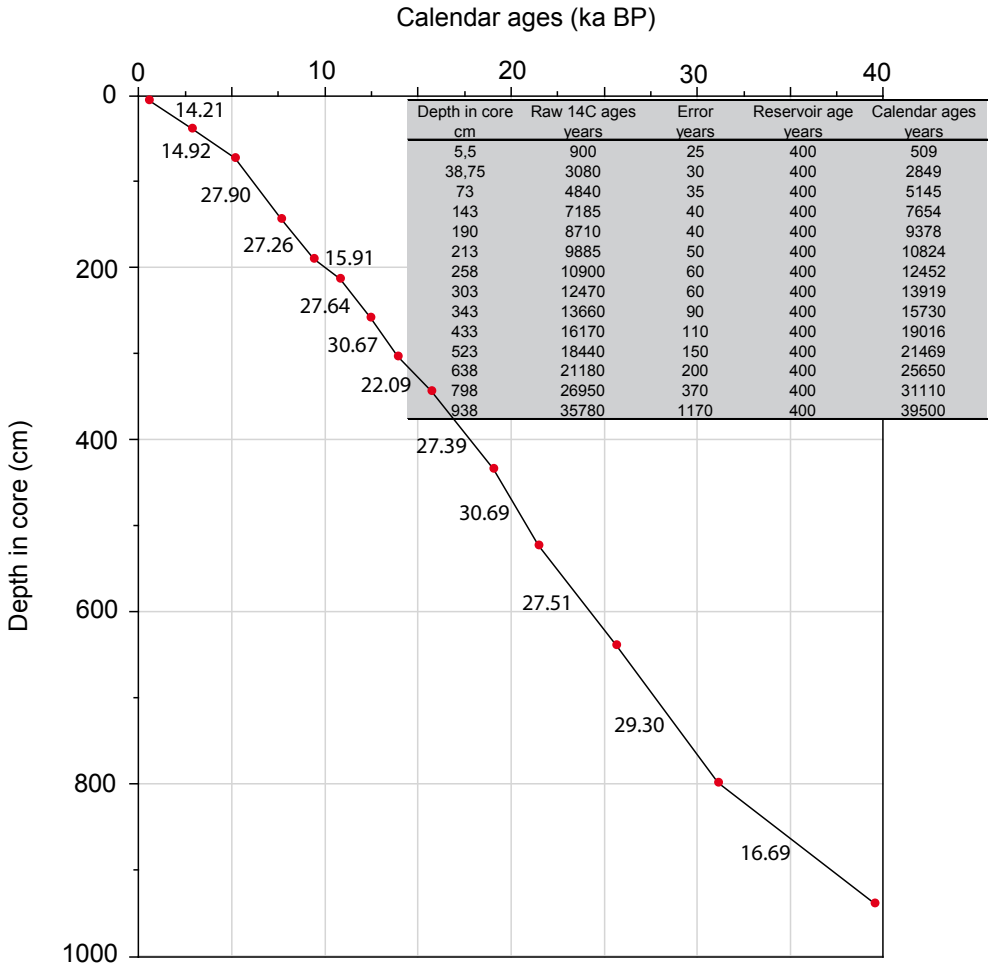

Depth in core cm	Raw 14C ages years	Error years	Reservoir age years	Calendar ages years
5,5	900	25	400	509
38,75	3080	30	400	2849
73	4840	35	400	5145
143	7185	40	400	7654
190	8710	40	400	9378
213	9885	50	400	10824
258	10900	60	400	12452
303	12470	60	400	13919
343	13660	90	400	15730
433	16170	110	400	19016
523	18440	150	400	21469
638	21180	200	400	25650
798	26950	370	400	31110
938	35780	1170	400	39500

Fig. 2. Age model of core GeoB4905-4. The table details the different steps taken to develop an age-model from raw 14C dates to calibrated ages. The graph depicts calibrated ages versus depth. The line depicts the linear interpolation between two consecutive ages. Age model of core GeoB4905-4 was previously published in Adegbie et al. (2003) and Weldeab et al. (2005). More details can be found therein. Numbers associated with the curve represent sedimentation rates in cm.ka-1.

Diatom accumulation rates were calculated with the following equation

$$\mathrm{DAR} = (N_\mathrm{v} \times \mathrm{WBD} \times \mathrm{SR})/2 \quad (1)$$

Where DAR are the diatom accumulation rates in millions $\mathrm{cm}^{-2}\,\mathrm{ka}^{-1}$, N_v are the number of diatom valves per gram of dry sediment, WBD is the wet bulk density in $\mathrm{g\,cm}^{-3}$ measured on board and SR are the sedimentation rates in $\mathrm{cm\,ka}^{-1}$.

Diatom census counts were performed on the upper 932 cm of core GeoB4905-4 with a resolution of 4 cm from top to 372 cm and 8 cm from 372 cm to 932 cm, which provided a temporal resolution of 150–300 yr between 0.14–17 cal. ka BP and 200–400 yr between 17–31 cal. ka BP and ∼500 between 31–40 cal. ka BP.

3.3 Ecological significance of diatoms

Around 80 diatom species or species groups were identified in core GeoB4905-4. To simplify this large dataset, species sharing similar ecology were lumped together. Previous investigations on diatom distribution in surface water and in surface sediments from low latitude environments have demonstrated that it was indeed possible to combine diatom species in several groups, based on habitats and nutrients and SST requirements. Identification of diatom groups in previous investigations were based on simple comparison of relative abundances or statistical approaches (Schuette and Schrader, 1981; Pokras et Molfino, 1986; Treppke et al., 1996; Schrader and Sorknes, 1997; Romero et al., 2002, 2009; Romero and Hebbeln, 2003; Jiang et al., 2004; Abrantes et al., 2007). We here build on the publications cited above, summarized in Romero and Armand (2010), to identify three different marine water groups

and one benthic/brackish water group. Two additional diatom groups were identified according to diatom distribution in African rivers and lakes to account for freshwater diatoms and windblown diatoms (Servant-Vildary, 1978; Gasse, 1980a, b, 1986).

3.3.1 Marine diatoms

Oligotrophe diatoms thrive in warm, nutrient-poor surface oceanic waters where siliceous productivity is low. This group is here dominated by large and highly silicified centric diatoms such as *Azpeitia* spp., *Planktonellia sol*, *Pseudosolenia calcaravis* and *Rhizosolenia* spp., *Thalassiosira* spp. with lesser occurrence of pennate diatoms such as *Nitzschia* spp. and *Thalassionema bacillare* (Table 1).

Mesotrophe diatoms live in nutrient-rich coastal marine environments. This group tracks higher dissolved silica levels, higher siliceous productivity but low turbulence (no upwelling conditions). This group is here dominated by large and highly silicified centric diatoms such as *Actinocyclus* spp., *Actinoptychus* spp., *Coscinodiscus* spp., *Paralia sulcata* and the pennate species *Fragilariopsis doliolus* (Table 1). *Cyclotella* species, dominated here by *C. stylorum/litoralis* and *C. striata*, occur both in coastal marine and coastal brackish environments (Lange and Syversten, 1989). The record of *Cyclotella* spp. in core GeoB4905-4 resembles the record of mesotrophe diatoms (Fig. 3), indicating that the two groups may share similar ecological preferences in the study area. *Cyclotella* spp. were subsequently added into the mesotrophe group (Fig. 4).

Eutrophe diatoms are thriving in surface waters with high DSi concentrations and/or high rate of nutrient replenishment to sustain blooming conditions. This group is here dominated by resting spores *Chaetoceros Hyalochaete* spp. (CRS) and *Thalassionema nitzschioides* var. *nitzschioides* with accompanying occurrences of *Thalassionema nitzschioides* var. *claviformis* (Table 1). Such species are very abundant in upwelling systems, though they can reach high occurrences in any eutrophe environment where DSi and iron concentrations are sufficient (Armand et al., 2008). As modern oceanography argues against upwelling of deep waters in the eastern Gulf of Guinea (Stramma and England, 1999), we here associate these species to eutrophe surface waters whose DSi and iron content depend on the Sanaga River discharge.

3.3.2 Benthic and freshwater diatoms

Diatoms of the benthic group attach to a substratum (rocks, sand, mudflats, macrophytes, etc.) present in shallow, marine to brackish waters of coastal zones and river mouths. This group is here dominated by pennate diatoms and, more particularly, by marine species of the genus *Cocconeis* (Table 1). This group tracks transport from the coast and/or river mouth to the core site (Pokras, 1991).

Freshwater diatoms live in rivers and lakes beyond the marine influence. Their presence in the marine environments can be due to river discharge and/or wind transport, the importance of each transport agent been variable between regions. This issue had to be assessed before any paleointerpretation based on the downcore records of freshwater diatom assemblages in core GeoB4905-4 could be made.

Investigation of sediment traps and surface sediments in the western and eastern Equatorial Atlantic indicated that *Aulacoseira granulata* and *A. islandica* (planktonic diatoms) are the most abundant freshwater diatoms transported by winds, while small pennate diatoms (benthic diatoms) are only present as trace (Romero et al., 1999). Similarly, investigation of diatom assemblages in a dust collector located at Mbour, Senegal, indicated that *A. granulata* and *Hantzschia amphioxys* are the two dominant diatoms in eolian dust coming from central and northern Sahara, respectively (Skonieczny et al., 2011). It is worth noting that *H. amphioxys* is absent from the diatom assemblages in core GeoB4905-4, which agrees well with an origin from the central Sahara of the eolian dust reaching the eastern Gulf of Guinea (Stuut et al., 2005). On the other hand, high abundances of freshwater diatoms were observed off the mouth of the Congo River (Jansen et al., 1989) due to high occurrence of *Aulacoseira* spp. (Uliana et al., 2002). In core GeoB4905-4, we observed a strong anti-correlation between *Aulacoseira* spp. AR and pennate diatom AR ($R = 0,77$; $n = 158$), therefore suggesting different transport agents for these two groups. Additionally, *Aulacoseira* spp. relative abundances are much lower than that of pennate diatom (1–2 % and 5–7 % respectively, except during H1 and the YD when relative abundances were not significant due to very few diatom valves present), which is opposite to findings off the Congo Riven where *Aulacoseira* spp. is the main freshwater diatom. These results argue against a riverine transport agent for the presence of *Aulacoseira* in core GeoB4905-4, especially as this genus is highly silicified and should better survive dissolution and mechanical break up during wet tansport.

Raphid pennate diatoms *Fragilaria* spp. and *Navicula* spp. dominate here the benthic community of freshwater diatoms (Table 1). It has been proposed that this group generally tracks river input to the marine environment (Gasse et al., 1989; Romero and Hebbeln, 2003). In the present study, it tracks the Sanaga River discharge in the eastern Gulf of Guinea and, ultimately, represents a record of the continental climate. In opposition, *Aulacoseira* spp., and in lesser occurrence *Stephanodiscus* spp. (Table 1), has been proposed to record wind deflation and transport intensity to the eastern Gulf of Guinea (Romero et al., 1999; Gasse, 2000). It is worth noting that *Aulacoseira* spp. are extremely abundant in emerged sediments of the dessicated paleolake Tchad (Servant-Vildary, 1982), which is the main source of aeolian dust to the eastern Equatorial Atlantic (Gasse et al., 1989; Stuut et al., 2005). The rather good agreement

Table 1. List of diatom species or species groups included in the different groups. Diatom group identification and diatom species assignment are detailed in the text.

Oligotrophe diatoms	Mesotrophe diatoms	Eutrophe diatoms	Benthic marine/brackish diatoms	Raphid freshwater diatoms	Windblown freshwater diatoms
Alveus marinus	*Actinocyclus* spp.	*Chaetoceros Hyalochaete* resting spores	*Achnantes* spp.	*Fallacia pygmaea*	*Aulacoseira granulata*
Azpeitia africana	*Actinocyclus curvatulus*	*Thalassionema nizschioides* var. *capitula*	*Amphora* spp.	*Fragilaria construens*	*Aulacoseira gotzeana*
Azpeitia nodulifera	*Actinocyclus octonarius*	*Thalassionema nizschioides* var. *claviformis*	*Catenula* spp.	*Fragilaria parasitica*	*Stephanodiscus* spp.
Azpeitia tabularis	*Actinoptychus* spp.	*Thalassionema nizschioides* var. *nitzschioides*	*Cocconeis* spp.	*Fragilaria pinnata*	
Bacteriastrum spp.	*Actinoptychus senarius*		*Cocconeis distans*	*Navicula* spp.	
Chaetoceros Phaeoceros spp.	*Actinoptychus vulgaris*		*Cocconeis fluminensis*	*Rhopalodia* spp.	
Nitzschia spp.	*Asteromphalus* spp.		*Cocconeis placentula*	*Synedra* spp.	
Nitzschia bicapitata	*Biddulphia* spp.		*Cocconeis scutellum*		
Nitzschia braarudii	*Coscinodiscus* spp.		*Diploneis* spp.		
Nitzschia interruptestriata	*Coscinodiscus centralis*		*Eunotogramma* spp.		
Nitzschia sicula	*Coscinodiscus decrescens*		*Gomphonema* spp.		
Planktonellia sol	*Coscinodiscus radiatus*		*Opephora marina*		
Proboscia alata	*Cyclotella* spp.		*Pleurosigma* spp.		
Pseudosolenia calcaravis	*Cyclotella caspia*		*Surirella* spp.		
Rhizosolenia spp.	*Cyclotella striata*		*Trachyneis aspera*		
Rhizosolenia acuminata	*Cyclotella litoralis/stylorum*				
Rhizosolenia bergonii	*Cymatotheca* spp.				
Rhizosolenia clevei	*Fragilariopsis doliolus*				
Rhizosolenia setigera	*Hemidiscus cuneiformis*				
Roperia tessalata	*Paralia sulcata*				
Thalassionema bacillare	*Pseudo-Nitzschia* spp.				
Thalassionema frauenfeldii	*Trigonium* spp.				
Thalassionema nitzschioides var. *parva*					
Thalassiosira spp.					
Thalassiosira eccentrica					
Thalassiosira leptopus					
Thalassiosira oestrupii					
Thalassiothrix spp.					

between *Aulacoseira* spp. AR and phytoliths AR records ($R = 0.33$; $n = 158$), the latter ones mainly transported in the eastern Equatorial Atlantic by winds (Jansen et al., 1989; Romero et al., 1999; Abrantes et al., 2003; and references therein), further argue for an atmospheric transport agent for *Aulacoseira* spp.

3.4 Opal phytoliths analysis

Opal Phytoliths were fixed on permanent slides concomitantly to diatoms. Phytoliths were counted congruently to diatom census counts, and *n* specimens (0 minimum–13 maximum) were identified until diatom counts were completed. As such, the total number of phytoliths is dependent on the abundances of diatoms, as well as the abundances of opal phytoliths. Opal phytolith AR were calculated using the same formula than for diatoms.

Taxonomic identification of opal phytoliths followed the nomenclature of Bukry (1980) and Bremond et al. (2008).

3.5 Ecological significance of phytoliths

Different shapes of opal phytoliths, formed inside the short cells of grass epidermis, prevail in different grass subfamilies. As such, phytoliths can be used to infer changes in land vegetation cover. The Cross and Bilobate short cell types occur dominantly in the Panicoideae grass subfamily, the Saddle type mainly occur in the Chloridoieae grass subfamily, the Rondel and Trapezoiform polylobate types are mainly produced by the Pooideae grass subfamily (Bremond et al., 2008). The Cross, Bilobate and Saddle types are precipitated in C_4 grasses while Trapezoiform types are formed in C_3 grasses. In core GeoB4905-4, the opal phytolith assemblages are dominated by Cross and Bilobate types with minor occurrences of Saddle and Trapezoiform types.

Basically, opal phytoliths presence in marine sediments can be due to transport by rivers and winds. Phytoliths and freshwater diatoms in surface sediments in the Zaire fan region do not present the same temporal distribution. Phytoliths AR are maximal 700 km offshore, while freshwater diatom AR are maximal at the river mouth and decrease offshore (Jansen et al., 1989). This suggests a significant aeolian transport of opal phytoliths from the Namib desert to the ocean by southeast trade winds. Phytoliths were also found in aeolian dust collected at Mbour, Senegal (Skonieczny et al., 2011) along with *Aulacoseira* spp. and *Hantzschia amphioxys* and in sediment traps off western Africa (Romero et al., 1999). This information and the good agreement between the phytolith and the *Aulacoseira* gp records in core GeoB4905-4 (Fig. 3) argue for an aeolian origin of opal phytoliths in the eastern Gulf of Guinea.

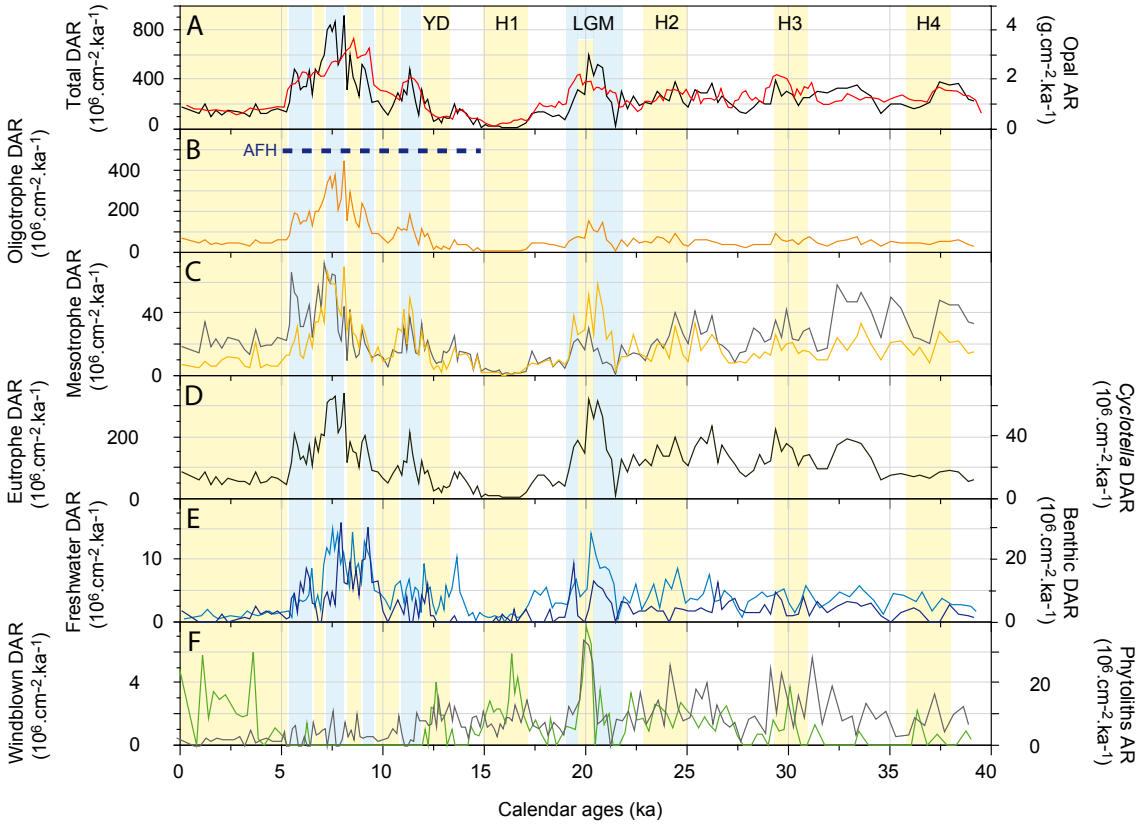

Fig. 3. Accumulation rates of diatoms and opal in core GeoB4905-4 versus calendar ages. **(A)** Total diatom accumulation rates (black line) and opal accumulation rates (red line), **(B)** accumulation rates of oligotrophe diatoms, **(C)** accumulation rates of mesotrophe diatoms (yellow line) and *Cyclotella* spp. (grey line), **(D)** accumulation rates of eutrophe diatoms, **(E)** accumulation rates of freshwater diatoms (light blue line) and benthic diatoms (dark blue line) and, **(F)** accumulation rates of *Aulacoseira* spp. (green line) and opal phytoliths (grey line). Blue and yellow shading represents periods of inferred high precipitations and low precipitations over western Africa, respectively.

3.6 Biogenic opal analysis

Opal was determined with the sequential leaching technique developed by Müller and Schneider (1993). Reproducibility of the data is below 2 %. Biogenic opal accumulation rates were calculated with the following equation

$$\text{OpalAR} = (\text{O} \times \text{WBD} \times \text{SR}), \quad (2)$$

where Opal AR is the opal accumulation rate in g cm^{-2} ka^{-1}, O is the opal content of the sediment, WBD is the wet bulk density in g cm^{-3} measured on board and SR is the sedimentation rate in cm ka^{-1}.

Part of the biogenic opal record (0–22 cal. ka BP) that has been used here to calculate opal AR was previously published by Weldeab et al. (2007).

4 Results

4.1 Biogenic opal

Biogenic opal AR varied between a minimum value of ∼0.2 g cm^{-2} ka^{-1} at 15–16 cal. ka BP and a maximum value of 3.5 g cm^{-2} ka^{-1} at 8–9 cal. ka BP (Fig. 3a, red line). Values were ∼1.5 g cm^{-2} ka^{-1}during the period between 40 cal. ka BP and 22 cal. ka BP and ∼2 g cm^{-2} ka^{-1}during the Last Glacial Maximum (LGM). Opal AR subsequently dropped to reach lowest values of ∼0.2 g cm^{-2} ka^{-1} between 17 cal. ka BP and 15 cal. ka BP, when they started to increase again. The increasing pattern between 15 cal. ka BP and 8 cal. ka BP was interrupted by two lows centred at ∼13 cal. ka BP and ∼10 cal. ka BP. Opal AR subsequently decreased slightly between 8 cal. ka BP and 6 cal. ka BP, when they abruptly dropped to values of ∼0.8 g cm^{-2} ka^{-1} that persisted during the last 5 cal. ka BP.

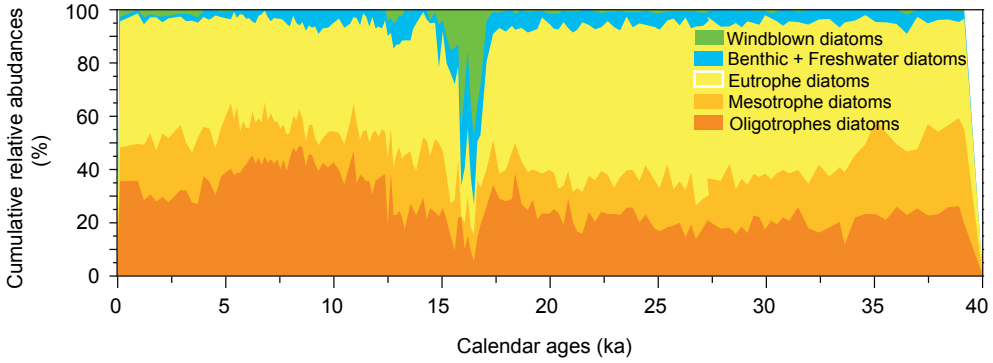

Fig. 4. Cumulative relative abundance of the five diatom groups in core GeoB4905-4 versus calendar ages.

4.2 Diatom and phytolith accumulation rates

Total diatom accumulation rates (DAR) present the same temporal pattern as opal AR during the last 40 cal. ka (Fig. 3a, black line). Values oscillated around 200.10^6 cm^{-2} ka^{-1} between 40 cal. ka BP and 22 cal. ka BP. Diatom AR increased to $\sim500.10^6$ cm^{-2} ka^{-1} during the LGM. Lowest diatom accumulation rates of $\sim10.10^6$ cm^{-2} ka^{-1} were observed during the 17–15 cal. ka BP period. Diatom AR increased again at 15 cal. ka BP to reach a maximum of $\sim850.10^6$ cm^{-2} ka^{-1} centred at 7.5 cal. ka BP. High DAR values were recorded until 5.7 cal. ka BP when they abruptly dropped to reach low values of $\sim150.10^6$ cm^{-2} ka^{-1} that persisted during the last 5 cal. ka. Millennial-scale events of low occurrences centred at 13 cal. ka BP, 10 cal. ka BP, 8.5 cal. ka BP and 6 cal. ka BP interrupted the period of highest DAR.

Oligotrophe diatoms presented very low AR between 40 cal. ka BP and 12.5 cal. ka BP, although a small increase occurred during the earliest phase of the LGM (Fig. 3b). Oligotrophe diatom AR presented values above $\sim100.10^6$ cm^{-2} ka^{-1} between 12.5 cal. ka BP and ~5 cal. ka BP. Highest DAR around 350.10^6 cm^{-2} ka^{-1} were recorded at ~7.5 cal. ka NP. Centennial-scale events of low occurrences centred at ~10 cal. ka BP, ~8.5 cal. ka BP and ~6 cal. ka BP interrupted the period of high accumulation rates of tropical diatoms. Very low AR values were again recorded since ~5 cal. ka BP.

Accumulation rates of mesotrophe diatoms (Fig. 3c, orange line), *Cyclotella* spp. (Fig. 3c, grey line) and eutrophe diatoms (Fig. 3d, yellow line) present a similar temporal pattern during the last 40 cal. ka BP as observed for total DAR (Fig. 3a, black line). It is worth noting that *Cyclotella* spp. are here dominated by marine-to-brackish *C. stylorum/litoralis* and *C. striata* (Table 1). Centennial-scale events of low AR centred at ~20 cal. ka BP, ~13 cal. ka BP, ~10 cal. ka BP, ~8.5 cal. ka BP and ~6 cal. ka BP are similarly apparent. Accumulation rates of mesotrophe diatoms, *Cyclotella* spp. and eutrophe diatoms presented variability of higher amplitude during the 40–18 cal. ka BP period than observed for total DAR and tropical diatom AR.

Accumulation rates of pennate freshwater (Fig. 3e, light blue line) and pennate marine benthic (Fig. 3e, dark blue line) diatoms co-vary during the last 40 cal. ka BP. They present low values until the LGM when they abruptly increased. A short-lived drop in AR of freshwater and benthic diatoms occurred at ~20 cal. ka BP. Accumulation rate values were low again between 18 cal. ka BP and 15 cal. ka BP when they started to increase to reach maximum values at ~7.5 cal. ka BP. Centennial-scale events of low occurrences centred at ~13 cal. ka BP, ~10 cal. ka BP, ~8.5 cal. ka BP and ~6 cal. ka BP interrupted the period of highest freshwater and benthic diatom AR.

Accumulation rates of windblown diatoms, represented by *A. granulata* and *A. gotzeana*, (Fig. 3f, green line) and opal phytoliths (Fig. 3f, grey line) present a similar evolution between 40 cal. ka BP and 4 cal. ka BP. Low AR values were generally observed throughout this period except during Heinrich Events (HE), a short-lived event centred at ~20 cal. ka BP and the Younger Dryas (YD). Low values were also observed during the 13–5 cal. ka BP period when highest DAR and opal AR were recorded. After 5 cal. ka BP, AR of windblown diatoms and phytoliths differ, with high occurrences of windblown diatoms and continuously low occurrences of opal phytoliths.

4.3 Diatom relative abundances

The relative contribution of each group to total diatom assemblages is depicted in Fig. 4. During the 40–35 cal. ka BP period, oligotrophe diatoms, mesotrophe diatoms and eutrophe diatoms amounted to ~95 % of the diatom assemblages, while freshwater and marine benthic diatoms accounted for ~5 %. Windblown diatoms were absent except for a short-lived occurrence at ~36 cal. ka BP. After 35 cal. ka BP, the contribution of oligotrophe diatoms decreased slightly, the contribution of mesotrophe diatoms decreased sharply (mainly because of less abundant *Cyclotella littoralis/stylorum*), while the contribution of

eutrophe diatoms increased. Freshwater and benthic diatoms were still present at low percentages, while windblown diatoms occurred episodically at percentages below 2 %.

An increase in both oligotrophe and mesotrophe diatoms was recorded between 22 cal. ka BP and 17.5 cal. ka BP at the expense of eutrophe diatoms. A very abrupt and pronounced decrease in marine diatoms occurred subsequently between 17.5 cal. ka BP and 15 cal. ka BP. During this period marine diatoms, produced locally, accounted for less than 50 % of the assemblage. The other fraction of the diatom assemblage was mainly represented by windblown diatoms with accompanying freshwater and benthic diatoms. However, the contribution of freshwater/benthic diatoms and windblown diatoms were out-of-phase during this event, as identified in the AR records (Fig. 3e and f). It is worth noting that less than 50 diatom valves per sample could be counted during this period and relative abundances are thus less significative. A second similar event, though much less pronounced, was observed between 12.5 cal. ka BP and 13.5 cal. ka BP. Here again, highest contribution of freshwater and benthic diatoms occurred just before and immediately after the peak abundance of windblown diatoms. Around 50-80 diatom valves per sample could be counted during this period.

Between 12.5 cal. ka BP and 5 cal. ka BP, the period of highest DAR in core GeoB4905-4, oligotrophe diatoms increased to account for ∼40 % of the diatom assemblages. Mesotrophe diatoms accounted for ∼10–15 %, while eutrophe diatoms decreased to ∼30 % of the diatom assemblage. Freshwater and benthic diatoms concomitantly represented ∼5–10 % of the assemblages, while windblown diatoms were totally absent. After ∼5 cal. ka BP, both oligotrophe and mesotrophe diatom abundances dropped, while abundances of eutrophe diatoms increased to ∼45 % of the assemblages. Freshwater and benthic diatoms almost disappeared, while windblown diatoms congruently increased to ∼3 % of the diatom assemblages.

5 Discussion

5.1 Diatom productivity during the last 40 cal. ka BP

The low variability range of sedimentation rates and sediment density values in core GeoB4905-4 (Fig. 2) indicates that variations in biogenic opal and total DAR reflect changes in siliceous productivity. Biogenic opal AR and DAR records demonstrated relatively low siliceous productivity during the 40–22 cal. ka BP period, high productivity during the LGM, low productivity during the 19–15 cal. ka BP period, high productivity during the 15–5.5 cal. ka BP and, eventually, low productivity since 5.5 cal. ka BP (Fig. 5a). Siliceous productivity was highest during the African Humid Period (AHP) as identified previously off Mauritania (deMenocal et al., 2000; Adkins et al., 2006) though processes driving productivity changes were there different. In core GeoB4905-4, variations in siliceous productivity over the last 40 cal. ka follow closely the variations in AR of freshwater (Fig. 3e, light blue line) and benthic (Fig. 3e, dark blue line) diatoms. The positive relationship between opal AR and freshwater/benthic diatom AR, and the fact that highest DAR and opal AR occurred during the AHP, suggest that diatom productivity in the eastern Gulf of Guinea was supported by strong DSi input through local rivers rather than due to a marine source. This agrees well with modern data demonstrating very low DSi content in the SACW (∼2.5 µM) that are transported into the eastern Gulf of Guinea by the GC and EUC (World Ocean Atlas, 2001) and high DSi content in local rivers (Boeglin et al., 2003; Hughes et al., 2011).

5.1.1 The Last Glacial Maximum

Diatom productivity was relatively high during the LGM, about half of the maximum siliceous productivity recorded during the early Holocene (Fig. 3). Diatom preservation was also good during the LGM. Mesotrophe and eutrophe diatoms dominated (Fig. 3c, orange line; Fig. 3d), while freshwater and benthic diatoms were half as abundant as during the early Holocene (Fig. 3e). Taken together, these results suggest that DSi input through local rivers was greater during the LGM than the rest of the last glacial and the early deglaciation. Greater DSi input could result from enhanced river discharges as a consequence of enhanced precipitation over the African continent or from a shift of the river mouths towards the core site during glacials due to sea level low stand. The extra pool of DSi was used by mesotrophe and eutrophe coastal diatoms. The cool SST (Fig. 5b) probably limited the development of oligotrophe subtropical diatoms despite large availability of DSi. The large peak in eutrophe diatoms, CRS and *T. nitzschioides* var. *nitzschioides*, generally dominant in coastal upwelling systems (Romero and Armand, 2011), may argue for the resurgence of subsurface waters during the LGM when the ITCZ migrated southwards, therefore strengthening northeast trade winds (Gasse et al., 2008). However, other windy but arid periods of the last 40 cal. ka BP, such as H1 and the YD (Multiza et al., 2008), conversely demonstrated lowest DAR in core GeoB4905-4 (Fig. 3). Subsurface waters transported into the eastern Gulf of Guinea are DSi-depleted (World Ocean Atlas, 2001) and resurgence of these waters could not support high diatom productivity during the LGM. This information supports our interpretation of a riverine origin of the DSi along the coast of Guinea.

5.1.2 The African Humid Period

We here use the generic term AHP despite that it might be inappropriate to properly describe the spatio-temporal heterogeneity of the timing of the onset and termination across the African continent (Kröpeling et al., 2008)

Diatom productivity started to increase at ∼15 cal. ka BP but was highest during ∼12 cal. ka BP and ∼5.5 cal. ka BP (Fig. 3). During this period, the AR of all diatom

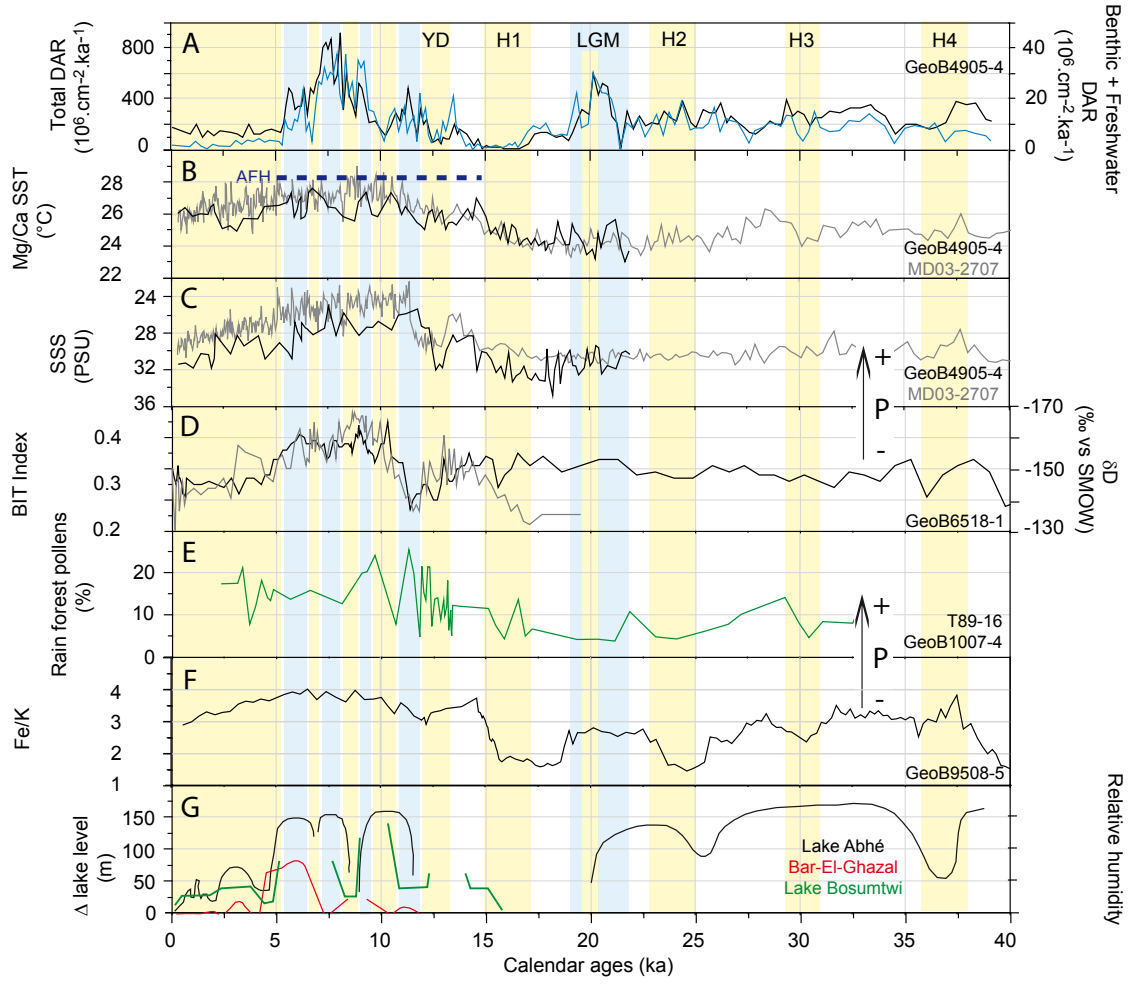

Fig. 5. Comparison of diatom and biogenic silica accumulation rates recorded in core GeoB4905-4 with climate proxies from Equatorial Africa. **(A)** Total diatom accumulation rates (black curve) and freshwater + marine/brackish benthic diatom accumulation rates (blue curve), **(B)** eastern Equatorial Atlantic sea-surface temperatures in core GeoB4905-4 (black line, Weldeab et al., 2007a) and in core MD03-2707 (grey line, Weldeab et al., 2007c), **(C)** eastern Gulf of Guinea sea-surface salinities in core GeoB4905-4 (black line, Weldeab et al., 2005) and in core MD03-2707 (grey line, Weldeab et al., 2007c), **(D)** BIT index tracing the input of continental organic carbon to the eastern equatorial Atlantic (black line, Weijers et al., 2009) and relative changes in central African humidity based on δD values of plant wax n-C_{29} alkanes (grey line, Schefuss et al., 2005), **(E)** proportion of lowland rainforest pollens in cores T89-16 and GeoB1007-4 (Marret et al., 2008), **(F)** elemental Fe/K ratio in core GeoB9508-5 off Senegal River (Mulitza et al., 2008), **(G)** lake level height above present level in Lake Abhe (11°05′ N–41°50′ E, black curve) and Bar-El-Ghazal (18° N 17° E, red curve) (Gasse, 2000) and relative humidity inferred from Lake Bosumtwi (green curve; Peck et al., 2004). *P*: inferred precipitations over western Equatorial Africa.

groups increased except for windblown diatoms and phytoliths. Again, the strong correlation between AR of freshwater diatoms and marine diatoms argue for a control of the siliceous productivity in the eastern Gulf of Guinea by injection of DSi by local rivers. During the AHP, enhanced precipitation over western Africa was the main driver of DSi input as deglacial sea level rise (Yokoyama et al., 2000) moved away river mouths from the core site. As such, diatoms in core GeoB4905-4 evidenced wettest conditions during ∼12 cal. ka BP and ∼5.5 cal. ka BP. This finding agrees well with previous studies carried out along the northwestern African coast (deMenocal et al., 2000; Adkins et al., 2006).

Greater availability of DSi during the AHP particularly favoured oligotrophe diatoms that increased by 20 % (Fig. 4) and from $\sim 0.10^6$ cm^{-2} ka^{-1} to $\sim 400.10^6$ cm^{-2} ka^{-1} since H1 (Fig. 3b). Conversely, relative abundances of eutrophe diatoms decreased during AHP though their AR increased from $\sim 0.5.10^6$ cm^{-2} ka^{-1} to $\sim 300.10^6$ cm^{-2} ka^{-1} since H1 (Fig. 3d). Eutrophe diatoms are fast blooming diatoms (Hargraves, 1972) thriving in coastal, nutrient-rich waters (Romero and Armand, 2010), while oligotrophe diatoms are slow-developing, large and heavily silicified diatoms thriving in warm surface waters (Romero et al., 1999). Today, the decreasing gradient in diatom abundances towards the western

Gulf of Guinea may indicate that marine coastal diatoms outcompete oligotrophe diatoms and uptake most of the DSi injected by rivers in the eastern Gulf of Guinea, thus preventing development of oligotrophe diatoms (Pokras and Molfino, 1986). Warmer SST during the early Holocene (Fig. 5b) may have been more favourable to oligotrophe subtropical diatoms that could extend their distribution and could make use of the higher DSi stocks.

5.1.3 The late Holocene

Diatom productivity was low again after the termination of the AHP at 5.5 cal. ka BP (Fig. 3). Since then, AR of all diatom groups decreased drastically, except for wind-blown diatoms, and relative abundances of eutrophe diatoms increased again (Fig. 4). Given Holocene sea level high stand, diatom counts suggest a reduction in the Sanaga River discharge, in agreement with drier and cooler conditions recorded elsewhere in sub-tropical North Africa (de Menocal et al., 2000; Adkins et al., 2006). The reduced pool of DSi injected by local rivers may have been readily used by marine coastal diatoms limiting westward diffusion, while lower SST (Fig. 5b) was unfavourable to oligotrophe subtropical diatoms. As a result, the relative abundances of eutrophe diatoms increased while that of oligotrophe diatoms decreased. Total diatom AR and assemblages did not show drastic changes since 5.5 cal. ka BP into the late Holocene, though a more detailed investigation of the last centuries would help to document how the recent warming of the ACT and greater precipitation over the coast of the Gulf of Guinea might have impacted diatom communities.

5.1.4 Millennial-scale events

Short lived drops in siliceous productivity, superimposed to the long trend, occurred during H1 and the YD, at ∼20 cal. ka BP during the LGM, ∼10 cal. ka BP, ∼8.5 cal. ka BP and ∼6 cal. ka BP during the AHP (Fig. 3). These drops probably represented short-term events of reduced DSi availability and, thus, sub-millennial periods of more arid conditions over western Equatorial Africa. Events of reduced diatom productivity were accompanied by large drops in oligotrophe diatoms (Fig. 3b), again indicating that most of the DSi may have been used by marine coastal diatoms. Diatom productivity was lowest during H1 and the YD. Diatom valves were greatly fragmented and dissolved, and diatom counts are not statistically significant. The poor preservation of diatom valves during H1 and YD further supports very low siliceous productivity in the eastern Gulf of Guinea during windy and arid periods identified in equatorial and tropical Africa (Gasse, 2000; Multiza et al., 2008).

5.2 Precipitation changes in western Equatorial Africa during the last 40 cal. ka BP

Given modern oceanography (Peterson and Stramma, 1991), modern relationship between chlorophyll-a standing stocks and the Sanaga River discharge (Weldeab et al., 2007a) and relationship between diatom distribution in core-top samples and riverine discharge in the eastern Gulf of Guinea (Jansen et al., 1989), diatom production is there mainly driven by DSi brought to the ocean by riverine freshwater discharge, which is dependent on precipitation changes in western Equatorial Africa. The diatom records from core GeoB4905-4 indicate that this scenario prevailed during the last 40 cal. ka, and that AR of raphid pennate diatoms (freshwater and marine/brackish benthic diatoms) can be used to infer past precipitation variations. The diatom records (Fig. 5a) demonstrate highest precipitation over western Equatorial Africa during the AHP, low precipitation during MIS3 and since 5.5 cal. ka BP and lowest precipitation during H1 and the YD. Short-lived dry spells occurred ∼10 cal. ka BP, ∼8.5 cal. ka BP and ∼6 cal. ka BP. interrupting wettest conditions of the AHP. The freshwater/benthic diatom signal might not track solely precipitation changes during the LGM because of the progradation of regional fluvio-deltaic systems during the last glacial as sea level dropped.

5.2.1 The Last Glacial Maximum

The diatom records in core GeoB4905-4 indicated that diatom productivity was relatively high during the LGM in relation to large input of DSi by local rivers. Both the shift of local river mouths towards the core site and/or the increase in precipitation could result in greater injection of DSi into the eastern Gulf of Guinea.

Large Pleistocene sediment deposits, created during the LGM lowest sea level stand, were observed at the modern shelf break, half way between core site and present day coastline (Giresse et al., 1995). These deposits indicated the presence of progradient fluvio-deltaic bodies towards the core site during the last glacial. During the LGM lowest sea level stand, the Ntem River appeared to be the main source of the terrigenous sediment deposited at the twin core MD03-2707 site (Weldeab et al., 2011), as the distance between the core site and the Ntem River outflow was greatly shortened. As such, higher freshwater diatom AR in core GeoB4905-4 during the LGM could result from the shortening of the distance between their source and their deposition site. The Ntem River contribution decreased rapidly since 19.8 cal. ka BP when sea level rose again, in phase with the drop in AR of freshwater and benthic diatoms.

The LGM is generally understood as a very dry period in western Equatorial Africa due to cold SST and atmospheric temperatures (Gasse et al., 2000; Lezine et al., 2005). However, few marine and terrestrial records from the Equatorial band studies indicated that the LGM may have been

wetter than MIS3 and H1 concomitant to greater with DAR in core GeoB4905-4 (Fig. 5a). SST records from GeoB4905-4 core (Weldeab et al., 2007a) and the twin core MD03-2707 (Weldeab et al., 2007c) showed a ∼1 °C surface water warming during the LGM compared to conditions prevailing just before and after (Fig. 5b). Reconstructed sea-surface salinities in core GeoB4905-4 (Weldeab et al., 2005) were ∼2 ‰ lower during the LGM than during H1. However, reconstructed sea-surface salinities in the twin core (Weldeab et al., 2007c) do not show any significant variations between 40 cal. ka BP and 17 cal. ka BP (Fig. 5c). Record of fluvial delivery in core GeoB6518-1 (Weijers et al., 2009), located at the mouth of the Congo River south of core GeoB4905-4, showed a small rebound during the LGM (Fig. 5d). Similarly, the Fe/K record in core GeoB9508-5 off Senegal (Mulitza et al., 2008) indicated moderate fluvial delivery during the LGM (Fig. 5f). Conversely, low resolution pollen records from two cores situated at the mouth of the Congo River (Marret et al., 2008) did not evidence any precipitation change during the 30–16 cal. ka BP period (Fig. 5e). Records from Lake Bosumtwi in Ghana evidenced lower dust load and higher organic content during the LGM than during H1 and the YD (Peck et al., 2004), arguing for wetter and less windy conditions during the LGM. A pollen record from Lake Barombi Mbo (western Cameroon) suggested a cloud-forest environment around the lake with a density comparable to the present during the period between 25 cal. ka BP and 20 cal. ka BP (Giresse et al., 1994). Lake Abhé (Ethiopia) depicted a drop in lake level during the middle part of the LGM (Gasse et al., 2008; Fig. 5g black line), while Lake Tila (northern Nigeria) suggested an increase in lake level at around 17 800 ^{14}C yr BP, i.e. 20.5 cal. ka BP (Salzmann et al., 2002), though radiocarbon date inversions preclude a precise age assignment. Finally, a high-resolution climate simulation (precipitation minus evaporation) at the LGM compared to the present showed a patch of increased effective moisture above the Sanaga drainage basin (Kim et al., 2008).

It is difficult to assess the respective impact of fluvio-deltaic system progradation and precipitation changes from a single record. However, our diatom data combined with existing paleo-records from Equatorial Africa suggest that land precipitations during the LGM may have been higher than during the MIS 3 and the early deglaciation until 12 cal. ka BP, and hence sufficient to promote moderate diatom production in the eastern Gulf of Guinea. Discrepancies between paleo-records from the southern part of the Gulf of Guinea, tracking precipitation changes in the Congo River drainage basin, and records from the northern part of the Gulf of Guinea and western north Africa, tracking precipitation changes in the Sanaga and Niger drainage basins, suggest different precipitation dynamics over the basins drained by the Congo and the Sanaga during the LGM or different impacts of Sanaga and Congo rivers discharges onto the marine environment. First, the Congo drainage basin is influenced by both the WAM and the East African Monsoon (Gasse, 2000; Tierney et al., 2011), while the Sanaga drainage basin is essentially influenced by the WAM. Second, southeastern trade winds promote a seasonal upwelling off the Congo River (Uliana et al., 2002; Marret et al., 2008) that does not occur in the eastern Gulf of Guinea. Enhanced upwelling during times of stronger trade winds generally intensified marine paleoproductivity in the Congo fan area during cold stages, but strongest river discharges also yield to upwelling of nutrient rich sub-surface waters during warm stages (Kim et al., 2010).

5.2.2 The African Humid Period

The diatom records from core GeoB4905-4 suggest an initiation of the AHP in western Equatorial Africa at 15 cal. ka BP (Fig. 5a) in phase with the first significant rise in SST in the eastern Gulf of Guinea (Fig. 5b) and early studies off Mauritania (deMenocal et al., 2000; Adkins et al., 2006). Diatom records also argue for a very gradual intensification of WAM rainfall between 15 cal. ka BP and 8 cal. ka BP, in agreement with the trend in local SST (Fig. 5b) but in opposition to a very abrupt onset of rainy conditions in subtropical North Africa (deMenocal et al., 2000; Adkins et al., 2006; Mulitza et al., 2008; Fig. 5f). The latter studies based their interpretations on terrigenous proxies tracking dust availability in the desert region of subtropical North Africa, which may respond faster to precipitation changes than DSi stocks and river discharge in Equatorial woodland regions. Our results also agree with a previous reconstruction, based on εNd data in core MD03-2707, identifying that the rainfall front of the WAM crossed the Sanaga drainage basin at 15 cal. ka BP (Weldeab et al., 2011). Between 11.5 cal. ka BP and 5 cal. ka BP, sea-surface salinities in eastern Gulf of Guinea were lowest (Fig. 5b), riverine discharges by western Equatorial African rivers were greatest (Fig. 5d and f), rain forest was more extended (Fig. 5e) and lake levels in Equatorial and northern subtropical Africa were highest (Fig. 5g). These results demonstrate that the WAM was not only more intense during the AHP but also reached its northernmost latitudinal position.

The termination of the AHP appears gradual in core GeoB4905-4, with a two-step reduction in precipitation from 7.5 cal. ka BP to 6.5 cal. ka BP and a final weakening of rainfall at ∼5.5 cal. ka BP, while termination of high precipitation conditions was much more abrupt, though synchronous, off Mauritania (deMenocal et al., 2000; Adkins et al., 2006). Our result may indicate a weakening of the WAM since 7.5 cal. ka BP, though the latitudinal range of the rain belt was probably the same until 5.5 cal. ka BP when the onset of the southward movement of the rainfall front began. As recorded by the total DAR, the termination of the AHP was in phase with the cooling of surface waters in the eastern Gulf of Guinea (Fig. 5b), increase of sea-surface salinity (Fig. 5c), decrease of riverine input (Fig. 5d) and large

drop in lake levels (Fig. 5g). Such dynamics for a gradual strengthening of the AHP between 15 cal. ka BP and 8 cal. ka BP, maximum intensity and extent of the WAM during the early Holocene and a gradual termination of the WAM between 7.5 cal. ka BP and 5.5 cal. ka BP is also supported by model output (Timm et al., 2010).

5.2.3 Millennial-scale events

The diatom records from core GeoB4905-4 and other marine and terrestrial records from the Equatorial band demonstrate that H1 was the driest period in western Africa during the last 40 cal. ka BP (Fig. 5). Increase in AR of windblown diatoms and opal phytoliths between 17 cal. ka BP and 15 ka BP (Fig. 3f) indicated concomitant windy conditions in agreement with the high dust loads recorded in Lake Tila during H2, H1 and the YD (Peck et al., 2004). The YD was the second driest period of the last 40 cal. ka BP (Fig. 5a). Dry conditions and low Sanaga River discharge are also reflected by the 4 ‰ increase in sea-surface salinity records from cores GeoB4905-4 (Weldeab et al., 2005) and MD03-2707 (Weldeab et al., 2007c) (Fig. 5c) and the decrease in Congo River delivery (Weijers et al., 2009; Fig. 5d). A phase lag of ∼500 yr is present between records from core GeoB4905-4 and records from cores located at the mouth of the Congo River. Disregarding dating uncertainties (∼200 yr in each core during the deglaciation), this phase lag may again indicate different precipitation dynamics over the two drainage basins during southward and northward migrations of the WAM and associated rainfall belt (Weldeab et al., 2011). Age model constrains do not allow, however, presenting a more accurate comparison and a further discussion on this issue.

The diatom records indicate that the AHP was interrupted by three prominent desiccation events centred at ∼10 cal. ka BP, ∼8.5 cal. ka BP and 6.5 cal. ka BP (Fig. 5a). Except for the 8.2 cal. ka BP event, these millennial scale events are not well expressed in the SST and SSS records from the eastern Gulf of Guinea (Fig. 3c and d), but are evident in records of African lake levels (Fig. 3g). Low AR of windblown diatoms and phytoliths during these rapid events (Fig. 3f) suggest that trade winds intensity did not change congruently. Within dating accuracy, the 8.5 cal. ka BP event evidenced in the diatom records of core Geob4905-4 may represent the well known 8.2 cal. ka BP event recognized worldwide (Alley and Agústsdóttir, 2005).

5.3 Forcing of precipitation changes in Equatorial Africa during the last 40 cal. ka BP

5.3.1 Long-term evolution

Precipitation changes over western Equatorial Africa at the precessional scale are controlled by the WAM. The quantity of moisture available for the WAM is partly determined by the SST gradient between tropics and subtropics and, thus, the presence and extent of the Atlantic Cold Tongue (ACT) in the subtropical south Atlantic (Thorncrof et al., 2011). Warm sea-surface temperature anomalies in the Gulf of Guinea lead to greater evaporation and water vapour in the lower troposphere that, in turn, conducts to greater precipitations along the Guinean Coast (Lebel et al., 2009). Historical observations of meteorological measurements along ships lanes in the Equatorial Atlantic have shown that the ACT weakened and warmed by 1.5 °C over the last sixty years (Tokinaga et al., 2011). This recent SST warming reduced southwesterly trade winds intensity and enhanced marine cloud cover over Equatorial Atlantic and land precipitation over western Equatorial Africa during the boreal summer season.

As it is difficult to unravel the impact of hydrographic modifications occasioned by glacial sea level drop and precipitation changes in western Equatorial Africa during the LGM, we here restrict the subsequent discussion to the last 20 000 yr. Based on the modern observations summarized above, we expect a causal relationship between SST in the eastern Equatorial Atlantic and precipitation regimes in western Equatorial Africa during the last 20 cal. ka BP (Fig. 5). We also expect a positive correlation between the SST record in core GeoB4905-4/MD03-2707 (Weldeab et al., 2007a, c) and our records of raphid freshwater and benthic/brackish diatom AR, and a negative correlation between the SST record and the records of windblown microfossils (Fig. 3). The SST records in core GeoB4905-4 and MD03-2707 (Fig. 5b) demonstrate a similar temporal evolution to DAR and freshwater/benthic diatom AR (Fig. 5a) over the last 20 cal. ka BP. Ocean temperatures were slightly higher during the LGM than the surrounding H2 and H1 and subsequently increased gradually to reach a maximum during 10 cal. ka BP and 5.5 cal. ka BP when they started dropping again. Variations in SST and intensity/extent of the ACT in the eastern Gulf of Guinea, forced by insolation changes at northern low latitudes (Weldeab et al., 2007c), may have been pivotal to drive precipitation changes on the Guinean coast. At a larger scale, additional processes are needed to explain the amplitude/extent and dynamics of the WAM since the LGM. Climate-vegetation models identified Northern Hemisphere deglaciation and vegetation-albedo-precipitation feedbacks to enhance the intensity/extent of the monsoon and dictate the precessional evolution of the WAM over the last 20 cal. ka BP: a rapid onset between 14.5 cal. ka BP and 11 cal. ka BP, a gradual increase until 9 cal. ka BP, a maximum in intensity/extent between 9 cal. ka BP and 7 cal. ka BP and a gradual reduction of moisture transport and a southward migration of the ITCZ since then (Timm et al., 2010), in agreement with the diatom records in core GeoB4905-4.

5.3.2 Millennial-scale events

Millennial-scale events identified in the diatom records from core GeoB4905-4 and other records from Equatorial Atlantic

and Equatorial Africa occurred under different mean climate states but may have rather similar origin.

The dry events identified during the LGM, H1 and the YD (Fig. 5a) were concomitant to pronounced sea-surface cooling in the eastern Gulf of Guinea (Fig. 5b; Weldeab et al., 2007a), which reduced moisture availability to the WAM. High AR of windblown diatoms during these periods argues for more intense atmospheric circulation that could allow for the spreading of the ACT. Climate modeling suggested that such temperature cooling, enhanced atmospheric circulation and precipitation reduction was induced by a southward shift of the ITCZ in conjunction with an intensification and southward expansion of the midtropospheric African Easterly Jet in response to a weakening of the Atlantic Meridional Overturning Circulation (AMOC) (Mulitza et al., 2008).

Millennial-scale events of reduced precipitation interrupting the AHP (Fig. 5a) are concomitant to small drops in eastern Equatorial Atlantic SST (Fig. 5b; Weldeab et al., 2005). Low windblown diatom AR (Fig. 3f) indicates no congruent intensification of the atmospheric circulation and therefore no significant extension of the ACT. These millennial-scale events are also synchronous to Bond's events 4, 5 and 7 (Bond et al., 1997), suggesting a possible relationship between Holocene AMOC reduction and dry AHP events through the atmospheric and oceanic teleconnections identified for the last glacial (Mulitza et al., 2008).

Millennial-scale events interrupting the Holocene warm mean state appear less intense than the ones scattering the glacial mean state, suggesting that both the initial mean state and the amplitude of AMOC reduction are important to dictate precipitation changes in western Equatorial Africa at this time scale.

6 Conclusions

Analyses of diatom assemblages in core GeoB4905-4 demonstrate that siliceous productivity changes in the eastern Gulf of Guinea during the last 40 cal. ka BP was controlled by both the dissolved silica delivered by local rivers to the ocean and sea-surface temperatures. Nutrient delivery was controlled by river discharges (precipitation forcing) or position/distance of river mouths relative to the core site (sea level forcing). The latter process may have been especially important during the LGM when sea level was lowest.

Precipitation over Equatorial Africa was more intense during the 15–5 cal. ka BP period (the so-called African Humid Period) though centennial-to-millennial timescale dry events were observed at ∼13 cal. ka BP, ∼10 cal. ka BP, ∼8.5 cal. ka BP and ∼6 cal. ka BP. The LGM may have been relatively wet in the Sanaga River drainage basin, though it was interrupted by a 1500 yr dry event centred at ∼20 cal. ka BP. Especially dry conditions occurred during H1, the YD and since 5.5 cal. ka BP as evidenced by the presence of windblown diatoms and phytoliths in the core during these intervals. Precipitation changes were linked to variations in the west African monsoon regime, forced locally by variations in intensity and extent of the Atlantic cold Tongue and distally by changes in Northern Hemisphere climate. Warmer sea-surface temperatures and greater discharge of dissolved silica during the early Holocene promoted the development of oligotrophe subtropical diatoms at the expense of eutrophe coastal diatoms. Oligotrophe diatoms are large and highly silicified, and their export to the sediment resulted in the high opal accumulation during the African Humid Period.

Acknowledgements. We thank Bruno Malaizé for constructive discussions and Fabienne Marret for data. We also thank Syee Weldeab and two anomymous reviewers for helpful comments that improved the manuscript. CX was funded by CNRS (Centre national de la Recherche Scientifique), OER was partially supported by CSIC (Spanish Research Council) and RS was funded by DFG (Deutsche Forschungsgemeinschaft). This is an EPOC contribution No. 1846.

Edited by: M. Siddall

The publication of this article is financed by CNRS-INSU.

References

Abrantes, F.: A 340,000 year continental record from tropical Africa – News from opal phytoliths from the equatorial Atlantic, Earth Planet. Sci. Lett., 209, 165–179, 2003.

Abrantes, F., Lopes, C., Mix, A., and Pisias, N.: Diatoms in southeast Pacific surface sediments reflect environmental properties, Quaternary Sci. Rev., 26, 155–169, 2007.

Adegbie, A. T., Schneider, R. R., Röhl, U., and Wefer, G.: Glacial millennial-scale fluctuations in central African precipitation recorded in terrigenous sediment supply and freshwater signals offshore Cameroon, Palaeogeogr. Palaeocl., 197, 323–333, 2003.

Adkins, J., deMenocal, P., and Eshel, G.: The "African Humid Period" and the record of marine upwelling from excess ^{230}Th in Ocean Drilling Program Hole 658C, Paleoceanography, 21, PA4203, doi:10.1029/2005PA001200, 2006.

Alley, R. B. and Agústsdóttir, A. M.: The 8k event: Cause and consequences of a major Holocene abrupt climate change, Quaternary Sci. Rev., 24, 1123–1149, 2005.

Boeglin, J. L., Ndam, J. R., and Braun, J. J.: Composition of the different reservoir waters in a tropical humid area: Example of the Nsimi catchment (Southern Cameroon), J. Afr. Earth Sci., 37, 103–110, 2003.

Armand, L. K., Cornet-Barthaux, V., Mosseri, J., and Quéguiner, B.: Late summer diatom biomass and community structure on

and around the naturally iron-fertilsed Kerguelen Plateau in the Southern Ocean, Deep-Sea Res. PT II, 55, 653–676, 2008.

Bond, G., Showers, W., Cheseby, M., Lotti, R., Almasi, P., deMenocal, P., Priore, P., Cullen, H., Hajdas, I., and Bonani, G.: A pervasive millennial-scale cycle in North Atlantic Holocene and glacial climates, Science, 278, 1257–1266, 1997.

Bremond, L., Alexandre, A., Wooller, M. J., Hély, C., Williamson, D., Schäfer, P. A., Majule, A., and Guiot, J.: Phytolith indices as proxies of grass subfamilies on East African tropical mountains, Global Planet. Change, 61, 209–224, 2008.

Bukry, D.: Opal phytoliths from the tropical eastern Pacific Ocean, Deep Sea Drilling Project Leg 54, in: Initial Rep. Deep Sea, edited by: Rosendahl, B. R. and Hekinian, R., US Govt. Printing Office, Washington, D. C, 575–590, 1980.

Crosta, X. and Koç, N.: Diatoms: From micropaleontology to isotope geochemistry, in: Proxies in Late Cenozoic Paleoceanography, edited by: Hilaire-Marcel, C. and de Vernal, A., Elsevier, Amsterdam, The Netherlands, 327–369, 2007.

Crosta, X., Pichon, J. J., and Labracherie, M.: Distribution of Chaetoceros resting spores in modern peri-Antarctic sediments, Mar. Micropaleontol., 29, 238–299, 1997.

deMenocal, P., Ortiz, J., Guilderson, T., Adkins, J., Sarnthein, M., Baker, L., and Yarusinsky, M.: Abrupt onset and termination of the African Humid Period: Rapid climate responses to gradual insolation forcing, Quaternary Sci. Rev., 19, 347–361, 2000.

Dürr, H. H., Meybeck, M., Hartmann, J., Laruelle, G. G., and Roubeix, V.: Global spatial distribution of natural riverine silica inputs to the coastal zone, Biogeosciences, 8, 597–620, doi:10.5194/bg-8-597-2011, 2011.

Foley, J. A., Coe, M. T., Scheffer, M., and Wang, G.: Regime shifts in the Sahara and Sahel: Interactions between ecological and climatic systems in Northern Africa, Ecosystems, 6, 524–539, 2003.

Gasse, F.: Les diatomées lacustres plio-pléistocène du Gadeb (Ethipie). Systématique, paléoécologie, biostratigraphie, Revue d'Algologie, Mémoire Hors-Série, 3, pp. 249, 262 pls, 1980a.

Gasse, F.: East African diatoms: Taxonomy, ecological distribution. J. Cramer, Berlin, Germany, pp. 201, 44 pls., 1980b.

Gasse, F.: Hydrological changes in the African tropics since the Last Glacial Maximum, Quaternary Sci. Rev., 19, 189–211, 2000.

Gasse, F., Stabell, B., Fourtanier, E., and van Iperen, Y.: Freshwater diatom influx in intertropical Atlantic: Relationhsips with continental records from Africa, Quaternary Res., 32, 229–243, 1989.

Giresse, P., Maley, J., and Brenac, P.: Late Quaternary palaeoenvironments in the Lake Barombi Mbo (West Cameroon) deduced from pollen and carbon isotopes of organic matter, Palaeogeogr. Palaeocl., 107, 65–78, 1994.

Giresse, P., Aloisi, J. C., Kuete, M., Monteillet, J., and NGueutchoua, G.: Quaternary sedimentary depositis on the Cameroon shelf : Characterization of facies and Late Quaternary shorelines, Quaternary Int., 29/30, 75–87, 1995.

Hargraves, P. E.: Studies on marine plankton diatoms. I. Chaetoceros diadema (Ehr.) Gran: life ecycle, structural morphology, and regional distribution, Phycologia, 11, 205–215, 1972.

Hasle, G. R. and Syversten, E. E.: Marine diatoms, in: Identifying Marine Diatoms and Dinoflagellates, edited by: Tomas, C. R., Academic Press, San Diego, USA, 5–385, 1997.

Hildebrand, M.: Silicic acid transport and its contron during cell wall silicification in diatoms, in: Biomineralization – From biology to biotechnology and medical applications, edited by: Baüerlein, E., Wiley-VCH, Weinheim, Germany, 170–188, 2000.

Hughes, H. J., Sondag, F., Cocquyt, C., Laraque, A., Pandi, A., André, L., and Cardinal, D.: Effect of seasonal biogenic silica variations on dissolved silicon fluxes and isotopic signatures in the Congo River, Limnol. Oceanogr., 556, 551–561, 2011.

Jansen, J. H. F., Alderliesten, C., Houston, C. M., Dejong, A. F. M., Vanderborg, K., and van Iperen, J. M.: Aridity in equatorial Africa during the last 225,000 years – A record of opal phytoliths/fresh-water diatoms from the Zaire (Congo) deep-sea fan (Northeast Angola Basin), Radiocarbon 31, 557–596, 1989.

Jiang, H., Zheng, Y., Ran, L., and Seidenkrantz, M.S.: Diatoms from the surface sediments of the South China sea and their relationships to modern hydrography, Mar. Micropaleontol., 53, 279–292, 2004.

Kim, S. J., Crowley, T. J., Erickson, D. J., Govindasamy, B., Duffy, P. B., Lee, B. Y.: High-resolution climate simulation of the last glacial maximum, Clim. Dynam., 31, 1–16, 2008.

Kim, S. Y., Scourse, J., Marret, F., and Lim, D. I.: A 26,000-year integrated record of marine and terrestrial environmental change off Gabon, west equatorial Africa, Palaeogeog. Palaeocl., 297, 428–438, 2010.

Kossoni, A. and Giresse, P.: Interaction of Holocene infilling processes between a tropical shallow lake system (Lake Ossa) and a nearby river system (Sanaga River) (South Cameroon), J. Afr. Earth Sci., 56, 1–14, 2010.

Kröpelin, S., Vershuren, D. Lézine, A. M., Eggermont, H., Cocquyt, C., Francus, P., Cazet, J. P., Rumes, B., Russell, J. M., Darius, F., Conley, D. J., Schuster, M., von Suchodoletz, H., and Engstrom, D. R.: Climate-driven ecosystem succession in the Sahara: The past 6000 years, Science, 320, 765–768, 2008.

Lange, C. B. and Syversten, E. E.: *Cyclotella litoralis* sp. nov. (Bacillariophyceae), and its relationships to *C. striata* and *C. stylorum*, Nova Hedwigia, 48, 341–356, 1989.

Lange, C. B. and Tiffany, M. A.: The diatom flora of the Salton Sea, California, Hydrobiologia, 473, 179–201, 2002.

Lebel, T. and Ali, A.: Recent trends in the Central and Western Sahel rainfall regime (1990–2007), J. Hydrol., 375, 52–64, 2009.

Lézine, A. M., Duplessy, J. C., and Cazet, J. P.: West African monsoon variability the last deglaciation and the Holocene: Evidence from fresh water algae, pollen and isotope data from core KW31, Gulf of Guinea, Palaeogeogr. Palaeocl., 219, 225–237, 2005.

Marret, F., Scourse, J., Kennedy, H., Ufkes, E., and Jansen, J. H. F.: Marine production in the Congo-influenced SE Atlantic over the past 30,000 years: A novel dinoflagellate-cyst based transfer function approach, Mar. Micropaleontol., 68, 198–222, 2008.

Martin-Jézéquel, V., Hildebrand, M., and Brzezinski, M. A.: Silicon metabolism in diatoms: Implications for growth, J. Phycol., 36, 821–840, 2000.

Moreno-Ruiz, J. L. and Licea, S.: Observations on the valve morphology of *Thalassionema nitzschoides* (Grunow) Hustedt, in: Proceedings of the 13th Symposium on Living and Fossil Diatoms, edited by: Marino, D. and Montresov, M., Biopress Limited Publisher, Bristol, Maretea, Italy, 1–7 September 1994, 393–413, 1994.

Moreno-Ruiz, J. L., Licea, S., and Santoyo, H.: Diatomeas del Golfo de California, Universidad Autonoma de Baja california Sur, Mexico, Mexico, pp. 203, 34 pls., 1996.

Mulitza, S., Prange, M., Stuut, J. B., Zabel, M., von Dobeneck, T., Itambi, A. C., Nizou, J., Schulz, M., and Wefer, G.: Sahel megadroughts trigerred by glacial slowdowns of Atlantic meridional overturning, Paleoceanography, 23, PA4206, doi:10.1029/2008PA001637, 2008.

Müller, P. J. and Schneider, R.: An automated leaching method for the determination of opal in sediments and particulate matter, Deep Sea-Res. PT I, 40, 425–444, 1993.

Peck, J. A., Green, R. R., Shanahan, T., King, J. W., Overpeck, J. T., and Scholz, C. A.: A magnetic mineral record of Late Quaternary tropical climate variability from lake Bosumtwi, Ghana, Palaeogeogr. Palaeocl., 215, 37–57, 2004.

Peterson, R. G. and Stramma, L.: Upper-level circulation in the South Atlantic Ocean, Progress in Oceanography, 26, 1–73, 1991.

Pokras, E. M.: A displaced diatom (*Delphineis karstenii*) in pelagic sediments of the southeast Atlantic, Mar. Micropaleontol., 17, 311–317, 1991.

Pokras, E. M. and Molfino, B.: Oceanographic control of diatom abundances and species distribution in surface sediment of the Tropical and Southeast Atlantic, Mar. Micropaleontol., 10, 165–188, 1986.

Ragueneau, O., Tréguer, P., Leynaert, A., Anderson, R. F., Brzezinski, M. A., DeMaster, D. J., Dugdale, R. C., Dymont, J., Fischer, G., François, R., Heinze, C., Maier-Riemer, E., Martin-Jézéquel, V., Nelson, D. M., and Quéguiner, B.: A review of the Si cycle in the modern ocean: Recent progress and missing gaps in the application of biogenic opal as a paleoproductivity proxy, Global Planet. Change, 26, 317–365, 2000.

Rathburn, A. E. and Deckker, P. D.: Magnesium and strontium compositions of recent benthic foraminifera from the Coral Sea, Australia and Prydz Bay, Antarctica, Mar. Micropaleontol., 32, 231–248, 1997.

Rivera, P., Cruces, F., and Avaria, S.: *Thalassionema bacillare* (Heiden) Kolbe (Thalassionemataceae, Bacillariophyceae): Una especia ahora casi desconocida para las aguas chilenas pero comun en el fitoplancton costero de la zona norte, Cienc. Tecnol. Mar., 29, 59–70, 2006.

Romero, O. E. and Armand L. K.: Marine diatoms as indicators of modern changes in oceanographic conditions, in: The diatoms: Applications for the Environmental an d Earth Sciences, edited by: Smol, J. P. and Stoermer, E. F., Second Edition, 373–400, 2010.

Romero, O. E. and Hebbeln, D.: Biogenic silica and diatom thanatocoenosis in surface sediments below the Peru-Chile Current: Controlling mechanisms and relationship with productivity of surface waters, Mar. Micropaleontol., 48, 71–90, 2003.

Romero, O. E., Lange, C. B., Fisher, G., Treppke, U. F., and Wefer, G.: Variability in export production documented by downward fluxes and species composition of marine planktic diatoms: Observations from the Tropical and Equatorial Atlantic, in: Use of Proxies in Paleoceanography: Examples from the South Atlantic, edited by: Fisher, G. and Wefer, G., Springer-Verlag, Berlin Heidelberg, Germany, 365–392, 1999.

Romero, O. E., Boeckel, B., Donner, B., Lavik, G., Fischer, G., and Wefer, G.: Seasonal productivity dynamics in the pelagic central Benguela system inferred from the flux of carbonate and silicate organisms, J. Mar. Syst., 37, 259–278, 2002.

Romero, O. E., Rixen, T., and Herunadi, B.: Effects of hydrographic and climatic forcing on diatom production and export in the tropical southeastern Indian ocean, Mar. Ecol. Progr. Ser., 384, 69–82, 2009.

Ruiz-Barradas, A., Carton, J. A., and Nigam, S.: Structure of interannual-to-decadal climate variability in the tropical Atlantic sector, J. Climate, 13, 3285–3297, 2000.

Salzmann, U., Hoelzmann, P., and Morczinek, I.: Late Quaternary climate and vegetation of the Sudanian Zone of Northeast Nigeria, Quaternary Res., 58, 73–83, 2002.

Sar, E. A., Sunesen, I., and Lavigne, A. S.: *Cymatotheca*, *Trybliptychus*, *Skeletonema* and *Cyclotella* (Thalassiosirales) from Argentinian coastal waters, Description of *Cyclotella cubiculata* sp. nov., Vie Milieu, 60, 135–156, 2010.

Shanahan, T. M., Overpeck, J. T., Wheeler, C. W., Beck, J. W., Pigati, J. S., Talbot, M. R., Scholz, C. A., Peck, J., and King, J. W.: Paleoclimatic variations in West Africa from a record of late Pleistocene and Holocene lake level stands of Lake Bosumtwi, Ghana, Palaeogeogr. Palaeocl., 242, 287–302, 2006.

Schefuss, E., Schouten, S., and Schneider, R.: Climatic controls on central African hydrology during the past 20.000 years, Nature, 437, 1033–1006, 2005.

Schrader, H. and Sorknes, R.: Peruvian coastal upwelling: Late Quaternary productivity changes revealed by diatoms, Mar. Geol., 97, 233–249, 1991.

Schuette, G. and Schrader, H.: Diatom taphocoenoses in the coastal upwelling area off south west Africa, Mar. Micropaleontol., 6, 131–155, 1981.

Servant-Vildary, S.: Etudes des diatomées et paléolimnologie du bassin tchadien au Cénozoique Supérieur, Travaux et Documents de l'ORSTOM, 84 (2 vol.), pp. 345, 1978.

Skonieczny, C., Bory, A., Bout-Roumazeilles, V., Abouchami, W., Galer, S. J. G., Crosta, X., Stuut, J. B., Meyer, I., Chiapello, I., Podvin, T., Chatenet, B., Diallo, A., and Ndiaye, T. : Mineral dust deposition multi-proxy characterization during a major Saharan spring outbreak, J. Geophys. Res., 116, D18210, doi:10.1029/2011JD016173, 2011.

Stramma, L. and England, M.: On the water masses and mean circulation of the South Atlantic Ocean, J. Geophys. Res., 104, 20863–20883, 1999.

Stuiver, M., Reimer, P. J., and Reimer, R. W.: CALIB 5.0, available at: http://calib.qub.ac.uk/calib/calib.html, last access: 6 March 2012, 2005.

Stuut, J. B., Zabel, M., Ratmeyer, V., Helmke, P., Schefuss, E., Lavik, G., and Schneider, R.: Provenance of present-day eolian dust collected off NW Africa, J. Geophys. Res., 110, D04202, doi:10.1029/2004JD005161, 2005.

Sundström, B. G.: The marine diatom genus *Rhizosolenia*. A new approach to the taxonomy, Ph.D. Thesis, University of Lund, Sweden, pp. 116, 39 pls., 1986.

Talbot, M. R. and Livingstone, D. A.: Hydrogen index and carbon isotopes of lacustrine organic matter as lake-level indicators, Palaeogeogr. Palaeocl., 80, 283–300, 1989.

Thorncroft, C. D., Nguyen, H., Zhang, C., and Peyrillé, P.: Annual cycle of the West African monsoon: Regional circulations and associated water vapour transport, Q. J. Roy. Meteor. Soc., 137 (Part A.), 129–147, 2011.

Tierney, J. E., Russell, J. M., Sinninghe Damsté, J. S., Huang, Y., and Verschuren, D.: Late Quaternary behavior of the East African monsoon and the importance of the Congo Air Bound-

ary, Quaternary Sci. Rev., 30, 798–807, 2011.

Timm, O., Köhler, P., Timmermann, A., and Menviel, L.: Mechanisms for the onset of the African Humid Period and Sahara greening 14.5–11 ka BP, J. Climate, 23, 2612–2633, 2010.

Tokinaga, H. and Xie, S.P .: Weakening of the equatorial Atlantic cold tongue over the past six decades, Nat. Geosci., 4, 222–226, 2011.

Tréguer, P., Nelson, D. M., van Bennekom, A. J., DeMaster, D. J., Leynaert, A., and Quéguiner, B.: The silica balance in the world ocean, Science, 268, 375–379, 1995.

Treppke, U. F., Lange, C. B., and Wefer, G.: Vertical fluxes of diatoms and silicoflagellates in the eastern equatorial Atlantic, and their contribution to the sedimentary record, Mar. Micropaleontol., 28, 73–96, 1996.

Uliana, E., Lange, C. B., and Wefer, G.: Evidence for Congo River freshwater load in Late Quaternary sediments of ODP Site 1077 (5° S, 10° E), Palaeogeogr. Palaeocl., 187, 137–150, 2002.

Weijers, J. W. H., Schefuss, E., Schouten, S., and Sinninghe Damsté, J. S.: Coupled thermal and hydrological evolution of the tropical Africa over the last deglaciation, Science, 315, 1701–1704, 2007.

Weijers, J. W. H., Schouten, S., Schefuss, E., Schneider, R. R., and Sinninghe Damsté, J. S.: Disentangling marine, soil and plant organic carbon contributions to continental margin sediments: A multi-proxy approach in a 20,000 year sediment record from the Congo deep-sea fan, Geochim. Cosmochim. Ac., 73, 119–132, 2009.

Weldeab, S., Schneider, R. R., Kölling, M., and Wefer, G.: Holocene African droughts relate to eastern equatorial Atlantic cooling, Geology, 33, 981–984, 2005.

Weldeab, S., Schneider, R. R., and Müller, P.: Comparison of Mg/Ca- and alkenone-based sea surface temperatures estimates in the fresh water-influenced Gulf of Guinea, eastern equatorial Atlantic, Geochem. Geophy. Geosy., 8, Q05P22, doi:10.1029/2006GC001360, 2007a.

Weldeab, S., Lea, D. W., Schneider, R. R., and Andersen, N.: Centennial scale climate instabilities in a wet early Holocene West African monsoon, Geophys. Res. Lett., 34, L24702, doi:10.1029/2007GL031898, 2007b.

Weldeab, S., Lea, D. W., Schneider, R., and Andersen, N.: 155.000 years of West African monsoon and ocean thermal evolution, Science, 316, 316–1307, 2007c.

Weldeab, S., Frank, M., Stichel, T., Haley, B., and Sangen, M.: Spatio-temporal evolution of the West African monsoon during the last deglaciation, Geophys. Res. Lett., 38, L13703, doi:10.1029/2011GL047805, 2011.

World Ocean Atlas 2001: Objective Analyses, Data Statistics, and Figures, CD-ROM documentation, US Dept. of Comm., Washington, D.C., 2001.

Yokoyama, Y., Lambeck, K., De Deckker, P., Johnston, P., and Fifield, L. K.: Timing of the Last Glacial Maximum from observed sea-level minima, Nature, 406, 713–716, 2000.